Inorganic Chemistry

Article

pubs.acs.org/IC

Magnetic and Luminescent Binuclear Double-Stranded Helicates

Paula Cucos,[†] Floriana Tuna,*[,‡] Lorenzo Sorace,*[,§] Iulia Matei,[⊥] Catalin Maxim,[†] Sergiu Shova,[∥] Ruxandra Gheorghe,[†] Andrea Caneschi,[§] Mihaela Hillebrand,[⊥] and Marius Andruh*[,†]

[†]Faculty of Chemistry, Inorganic Chemistry Laboratory, University of Bucharest, Str. Dumbrava Rosie no. 23, 020464 Bucharest, Romania

[‡]National EPR Research Facility, School of Chemistry and Photon Science Institute, University of Manchester, Oxford Road, Manchester, M13 9PL, U.K.

[§]Department of Chemistry "U. Schiff" and INSTM RU, University of Florence, Via della Lastruccia 3, 50019 Sesto Fiorentino (FI), Italy

[⊥]Department of Physical Chemistry, University of Bucharest, Bd. Regina Elisabeta 4-12, 030018 Bucharest, Romania

[∥]"Petru Poni" Institute of Macromolecular Chemistry, Aleea Grigore Ghica Voda 41A, RO-700487 Iasi, Romania

Supporting Information

ABSTRACT: Three new binuclear helicates, $[M_2L_2]\cdot 3DMF$ (M = Co(II), **1**, Zn(II), **3**) and $[Cu_2L_2]\cdot DMF\cdot 0.4H_2O$ (**2**), have been assembled using the helicand H_2L that results from the 2:1 condensation reaction between *o*-vanillin and 4,4′-diaminodiphenyl ether. The metal ions within the binuclear helicates are tetracoordinated with a distorted tetrahedral geometry. Direct current magnetic characterization and EPR spectroscopy of the Co(II) derivative point to an easy axis type anisotropy for both Co(II) centers, with a separation of at least 55 K between the two doublets. Dynamic susceptibility measurements evidence slow relaxation of the magnetization in an applied dc field. Since the distance between the cobalt ions is quite large (11.59 Å), this is attributed in a first instance to the intrinsic properties of each Co(II) center (single-ion magnet behavior). However, the temperature dependence of the relaxation rate and the absence of slow dynamics in the Zn(II)-doped sample suggest that neither the simple Orbach mechanism nor Raman or direct processes can account for the relaxation, and collective phenomena have to be invoked for the observed behavior. Finally, due to the rigidization of the two organic ligands upon coordination, the pure zinc derivative exhibits fluorescence emission in solution, which was analyzed in terms of fluorescence quantum yields and lifetimes.

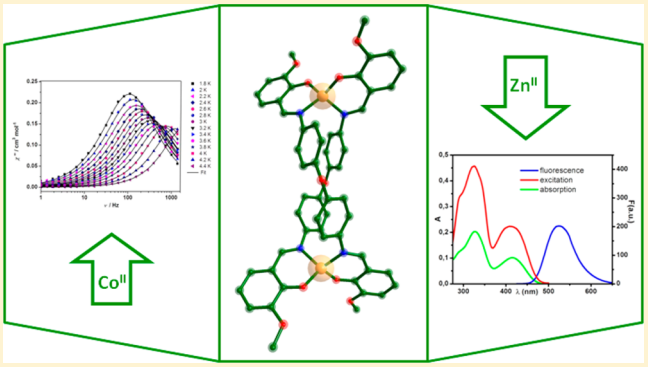

INTRODUCTION

The rational design of metallic helicates represents one of the early spectacular achievements of metallosupramolecular chemistry.[1] Several classes of organic molecules (helicands) were synthesized and used for the assembly of double- and triple-stranded homo- and heterometallic helicates, which have been recently reviewed in excellent papers.[2] The helicands are linear strands with repeating complexation sites separated by suitable spacers.[3] Numerous helicands are bis-Schiff bases derived from hydrazine (diazine ligands)[4] or long/rigid diamines.[4c,5] Among the azomethinic helicands, which are related to the present work, we mention the Schiff bases resulting from the 2:1 condensation between *o*-vanillin and various diamines.[6]

Apart from their beauty, the metallohelicates display exciting physical properties, such as luminescence and magnetism. There are two important types of luminescent helicates: those for which the light emission arises from the metallic centers (most frequently lanthanide cations),[7] and helicates owing their luminescence to the organic ligand, which becomes rigid upon coordination to the metal ions (for example Zn(II) ions).[8] From the magnetic point of view, the metal ions within a helical structure can interact with each other, when the distance between them is small and the bridging fragments are able to mediate the exchange interactions. If the metal ions are significantly separated, they behave independently from the magnetic point of view. In this last case two types of magnetic behaviors are particularly important: (i) the metal ions exhibit spin crossover phenomena;[5c,9] (ii) each metal ion shows slow relaxation of the magnetization; that is, it acts as a single-ion magnet (SIM).[10] Most of the helicates featuring SIM behavior are based on strongly anisotropic lanthanide cations. In this paper we report on three new binuclear helicates constructed using a Schiff-base helicand resulting from the condensation of *o*-vanillin with 4,4′-diaminodiphenyl ether. This organic

Received: May 7, 2014
Published: July 7, 2014

   dx.doi.org/10.1021/ic501051q | *Inorg. Chem.* 2014, 53, 7738−7747

Table 1. Selected Bond Lengths (Å) and Angles (deg) for Compounds 1−3

1		2		3	
Co(1)−O(7)	1.890(2)	Cu(1)−N(1)	1.978(6)	Zn(1)−O(2)	1.899(2)
Co(1)−O(8)	1.891(3)	Cu(1)−N(2)	1.979(5)	Zn(1)−O(3)	1.901(2)
Co(1)−N(3)	1.985(3)	Cu(1)−O(1)	1.883(4)	Zn(1)−N(1)	2.003(3)
Co(1)−N(4)	1.996(3)	Cu(1)−O(2)	1.902(5)	Zn(1)−N(2)	2.019(3)
Co(2)−O(3)	1.898(2)			Zn(2)−O(8)	1.901(3)
Co(2)−O(2)	1.898(2)	O(2)−Cu(1)−N(2)	92.8(2)	Zn(2)−O(7)	1.904(3)
Co(2)−N(1)	1.989(3)	N(1)−Cu(1)−N(2)	101.3(2)	Zn(2)−N(3)	1.997(3)
Co(2)−N(2)	1.990(3)	O(1)−Cu(1)−O(2)	87.8(2)	Zn(2)−N(4)	2.011(3)
Co(1)···Co(2)	11.590(6)	O(1)−Cu(1)−N(1)	94.4(2)	Zn(1)···Zn(2)	11.606(1)
O(7)−Co(1)−O(8)	116.13(12)			O(2)−Zn(1)−O(3)	110.89(11)
O(7)−Co(1)−N(3)	123.79(12)			O(2)−Zn(1)−N(1)	129.23(12)
O(8)−Co(1)−N(3)	95.37(11)			O(3)−Zn(1)−N(1)	95.87(11)
O(7)−Co(1)−N(4)	94.83(11)			O(2)−Zn(1)−N(2)	94.66(11)
O(8)−Co(1)−N(4)	121.98(12)			O(3)−Zn(1)−N(2)	123.59(13)
N(3)−Co(1)−N(4)	106.64(11)			N(1)−Zn(1)−N(2)	105.50(11)
O(3)−Co(2)−O(2)	112.72(11)			O(8)−Zn(2)−O(7)	114.31(13)
O(3)−Co(2)−N(1)	95.23(11)			O(8)−Zn(2)−N(3)	96.52(11)
O(2)−Co(2)−N(1)	126.51(12)			O(7)−Zn(2)−N(3)	123.54(12)
O(3)−Co(2)−N(2)	123.68(12)			O(8)−Zn(2)−N(4)	122.09(13)
O(2)−Co(2)−N(2)	94.51(12)			O(7)−Zn(2)−N(4)	95.36(11)
N(1)−Co(2)−N(2)	106.85(12)			N(3)−Zn(2)−N(4)	106.94(11)

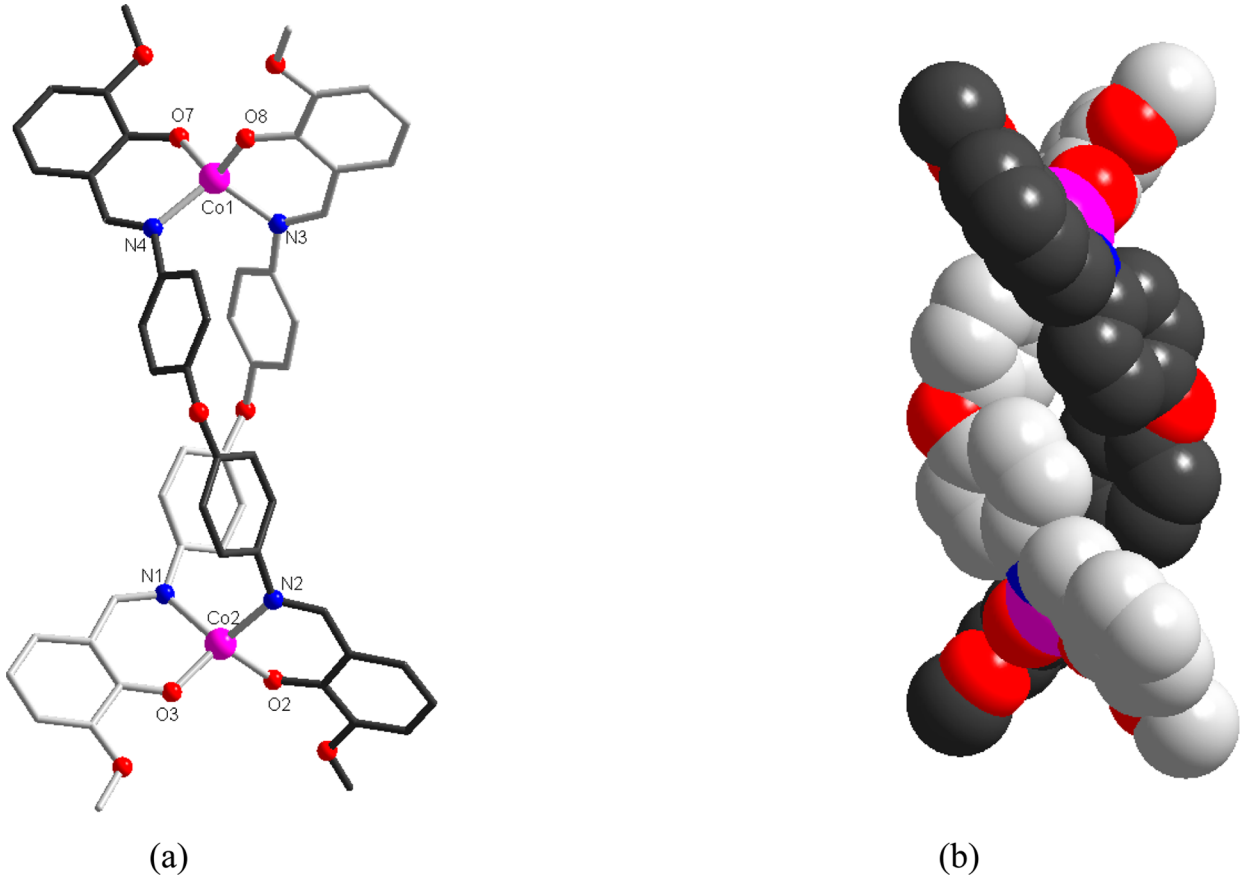

Figure 1. (a) View of the cobalt helicate **1** along with the atom-numbering scheme; (b) space-filling representation.

molecule was first reported and crystallographically characterized by Xu et al.[11] As assembling cations we employed Co(II), Cu(II), and Zn(II). The cobalt ion was chosen for its significant magnetic anisotropy, which makes it a good candidate to check the SIM behavior: indeed, a few tetrahedral complexes have been recently reported to show such behavior, as a consequence of either an easy axis or an easy plane anisotropy.[12]

The luminescence of the zinc derivative has been investigated in terms of fluorescence quantum yields, lifetimes, and spectral features, as a function of solvent polarity.

dx.doi.org/10.1021/ic501051q | Inorg. Chem. 2014, 53, 7738−7747

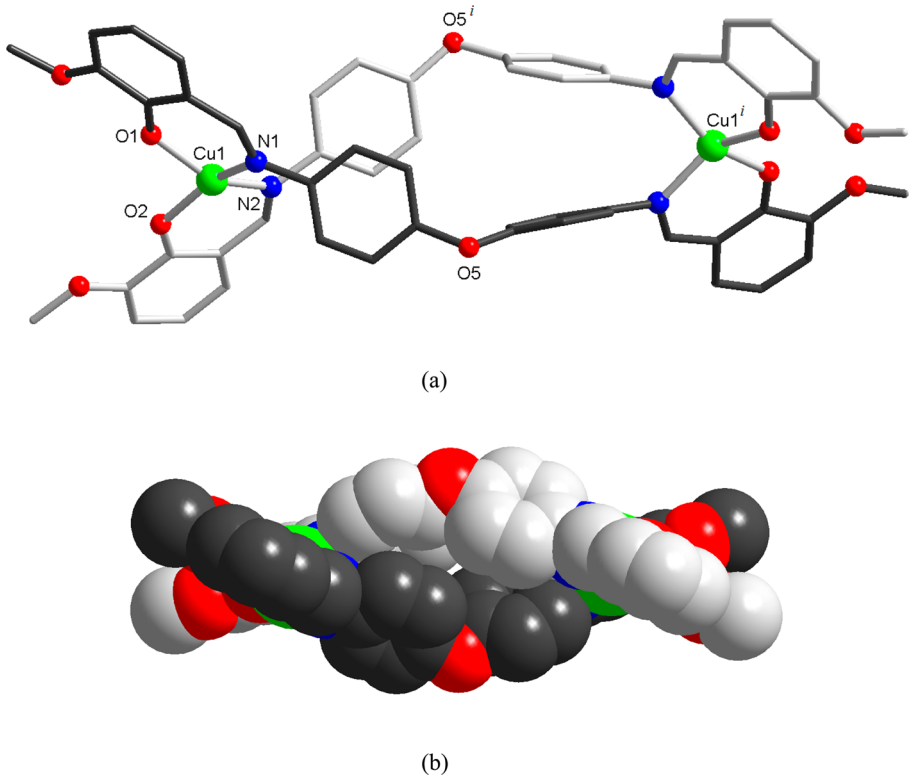

Figure 2. (a) View of the copper helicate **2** along with the atom-numbering scheme; (b) space-filling representation (^{i} = 1.5−*x*, 1.5−*y*, *z*).

RESULTS AND DISCUSSION

The new helicates result from the reaction of the deprotonated helicand, L^{2-}, with each of the three assembling cations: Co(II), Cu(II), and Zn(II), respectively: $[Co_2L_2]\cdot 3DMF$, **1**; $[Cu_2L_2]\cdot DMF\cdot 0.4H_2O$, **2**; $[Zn_2L_2]\cdot 3DMF$, **3**.

Description of the Structures. The crystal structures of the three compounds have been solved. Compounds **1** and **3** are isomorphous, whereas compound **2** crystallizes in a different unit cell; however, all the molecular structures are very similar. They consist of dinuclear double-stranded helicates, in which two ligand molecules wrap around the two metal ions. Since the space groups are centrosymmetric, the two enantiomers cocrystallize within the same single crystal. In the three compounds the metal ions are tetracoordinated. Selected bond distances and angles for compounds **1**−**3** are collected in Table 1. Let us discuss first the structure of compound **1** (Figure 1). The cobalt ions show a distorted tetrahedral geometry, being coordinated by two phenoxo oxygen and two imino nitrogen atoms arising from two helicands. The dihedral angles formed by the two ligands coordinated to Co1 and Co2 are respectively 80.32° and 77.32°. The Co−O distances for the two cobalt(II) ions vary between 1.890(2) and 1.898(2) Å, while the Co−N distances are slightly longer (1.985(3)−1.996(3) Å). The helical twists of the ligands, as defined by the torsion angles Co(1)−N(3)−N(1)−Co(2) and Co(1)−N(4)−N(2)−Co(2), are 147.9° and 138.7°, respectively. The intramolecular distance between the cobalt atoms is 11.59 Å. The molecular structure of **2** is presented in Figure 2. The main difference between the structures of **1** and **2** arises from the distortion degree of the coordination polyhedron, from the ideal tetrahedral geometry. The dihedral angle for the copper(II) ions in **2**, which are crystallographically equivalent, is much lower (44.00°) in comparison with the values found for the cobalt ions in **1**. The Cu−O distances (Cu1−O1 = 1.883(4); Cu1−O2 = 1.902(5) Å) are slightly shorter than the Cu−N ones (Cu1−N1 = 1.978(6); Cu1−N2 = 1.979(5) Å). The helical twist of the ligands is given by the torsion angle Cu(1)−N(1)−N(2)−Cu(1)^{i} = 135.1°, ^{i} = 1.5−*x*, 1.5−*y*, *z*. Intramolecular $\pi-\pi$ stacking interactions are established between the phenyl rings from the diphenyl ether moieties of the two helicands in **2** (centroid−centroid distance 3.89 Å, Figure S1). The phenyl rings within each pair are not parallel, the value of the dihedral between them being 18.48°. The corresponding distances in **1** are longer (4.26 Å), and the dihedral angles are 7.74° and 20.46°. The shortest intermolecular Co···Co distances between neighboring helicates are 7.915, 7.947, and 9.219 Å. The molecular structure of the zinc helicate, **3**, is very close to **1** and is presented in Figure S2.

Concerning the packing diagrams, the most interesting features are observed with compound **2**. Helicates with the same chirality are arranged in helicoidal supramolecular chains (Figure 3a), which are assembled through face-to-face $\pi-\pi$ stacking interactions established between the phenyl rings of *o*-vanillin fragments (centroid−centroid distance: 3.51 Å). The chains running in the same direction form layers. The chains from adjacent layers are perpendicular (Figure 3b). Their packing generates channels hosting the solvent molecules (Figure S3).

Magnetic Properties of the Cobalt(II) Helicate. The long distance between the cobalt(II) ions within helicate **1** prompted us to investigate the occurrence of slow relaxation phenomena for the individual metal ions, if any, for this compound. The cobalt(II) ion is known to show a significant magnetic anisotropy, which makes it a good candidate for constructing single-molecule magnets and single-chain magnets.[13] More recently, it has been shown that cobalt(II)

dx.doi.org/10.1021/ic501051q | *Inorg. Chem.* 2014, 53, 7738−7747

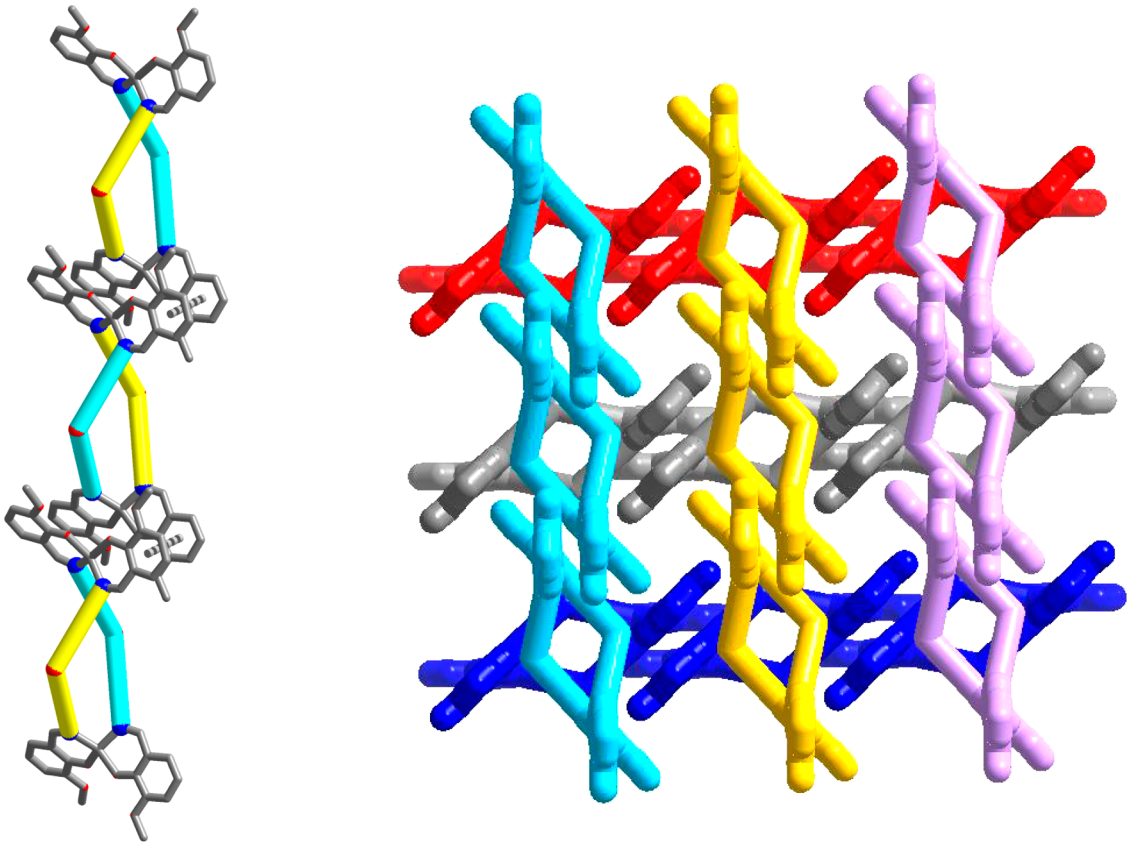

Figure 3. (a) Representation of a helical supramolecular chain assembled through $\pi-\pi$ stacking interactions for crystal **2** (the diphenylether moieties within helicates are differentiated by color); (b) detail of the packing diagram showing the formation of channels (supramolecular chains are differentiated by color). The diphenyl ether moieties are represented simplified in both pictures.

mononuclear complexes can act as single-ion magnets, but the number of such systems is limited to only a few examples.[12a,b,14] The $\chi_M T$ vs T curve for **1** is represented in Figure 4 (χ_M represents the magnetic susceptibility per cobalt(II) ion). The room-temperature value of the $\chi_M T$ product (2.4 cm^3 mol^{-1} K)

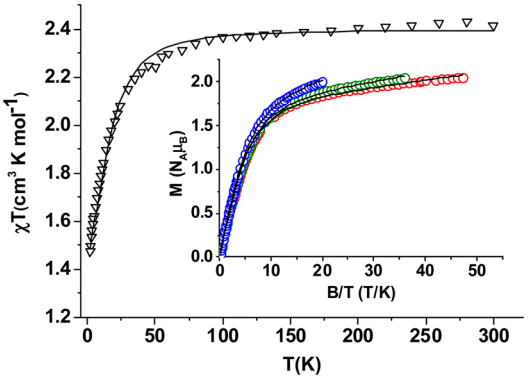

Figure 4. Temperature dependence of the $\chi_M T$ product for **1**, reported for Co(II) mole, together with best fit curve obtained by using parameters reported in the text. In the inset the reduced magnetization curves measured at 1.9 K (red circles), 2.5 K (green circles), and 4.5 K (blue circles) are plotted; continuous lines represent the best fit to experimental data using parameters reported in the text. The two models described in the text with $D < 0$ using axial or partially rhombic ZFS provide indistinguishable curves.

corresponds to the expected one for an independent tetrahedral Co^{II} ion ($S = 3/2$, $g = 2.26$). By decreasing the temperature, $\chi_M T$ remains constant down to 90 K; then it decreases smoothly, reaching 1.45 cm^3 mol^{-1} K at 2 K. Since the distance between the two cobalt(II) ions is long, any exchange interaction between them can be safely discarded or considered as a minor perturbation to the magnetic anisotropy effects. As a consequence, the decrease of $\chi_M T$ observed below 100 K was ascribed to zero field splitting (ZFS) of the $S = 3/2$ state. The field-dependent magnetization curves, measured at 1.9, 2.5, and 4.5 K up to 90 kOe, are in agreement with this interpretation, showing non-superimposable M vs H/T traces (inset in Figure 4). Accordingly, we fitted[15] both sets of data by using the Hamiltonian

$$\hat{\mathbf{H}}_{zfs} = D[\hat{S}_z^{\,2} - 1/3S(S+1)] + \mu_B \hat{\mathbf{S}}\cdot\mathbf{g}\cdot\hat{\mathbf{H}} \qquad (1)$$

where we neglected rhombic components of the ZFS to reduce overparametrization. The best fit to the M vs H data led to $g_\perp = 2.21(2)$, $g_\parallel = 2.36(2)$; $D = -29(3)$ cm^{-1}, while the $\chi_M T$ vs T data were best reproduced by $g_{iso} = 2.28(1)$; $|D| = 20(2)$ cm^{-1}. It is to be stressed that the latter fit is essentially insensitive to the sign of the D parameter, i.e., to the nature (easy axis or easy plane) of the magnetic anisotropy, whereas it turned out to be impossible to obtain a fit of reasonable quality for M vs H assuming $D > 0$ (see Figure S4). On the other hand, the use of an isotropic g factor and the inclusion of the rhombic term $E(\hat{S}_x^{\,2} - \hat{S}_y^{\,2})$ in eq 1 provided a fit of comparable quality, with

dx.doi.org/10.1021/ic501051q | Inorg. Chem. 2014, 53, 7738−7747

best fit parameters g_{iso} = 2.30(1), D = −34(4) cm^{-1}, and E/D = 0.09(2).

To get more information on this point, we performed EPR spectroscopy on **1**. The W-band ($\nu \approx 94$ GHz) spectrum, recorded at 10 K (Figure 5), clearly shows only a single,

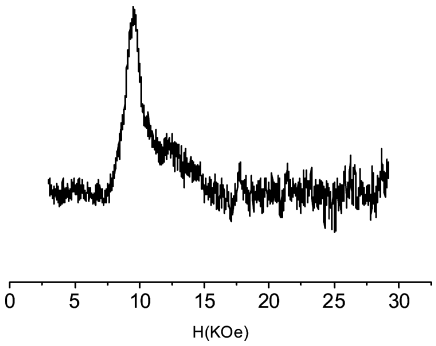

Figure 5. W-band (ν = 94.27 GHz) EPR spectrum of a microcrystalline powder sample of **1** measured at 10 K.

parallel-type transition occurring at an effective g value of g^{eff} = 7.05(5), while no sign of perpendicular-type transitions is observed. Interestingly, only one signal is observed, indicating that the small differences in the coordination sphere of the two cobalt centers are not enough to induce remarkable differences in their electronic structure. The observed spectrum clearly can be interpreted considering the ground doublet as an effective S = 1/2 and confirms the easy axis type anisotropy for both centers, since $g^{eff}_{\parallel} \gg g^{eff}_{\perp}$. Indeed, for an S = 3/2 with $D \gg h\nu$, a perturbative treatment provides the following relations between the effective and real g values and the zero field splitting parameters:[16]

$$g_x^{eff} = g_x\left(1 \pm \frac{1-3\lambda}{\sqrt{1+3\lambda^2}}\right)$$

$$g_y^{eff} = g_y\left(1 \pm \frac{1+3\lambda}{\sqrt{1+3\lambda^2}}\right)$$

$$g_z^{eff} = g_z\left(1 \mp \frac{2}{\sqrt{1+3\lambda^2}}\right) \quad (2)$$

where $\lambda = E/D$ and in each equation the upper sign is valid for a dominant $M_S = \pm 1/2$ doublet, while the lowest applies for a dominant $M_S = \pm 3/2$ doublet. It is immediately evident that the only possible way to observe an EPR signal at $g^{eff} \approx 7$ is to assume $g_z > 2.33$ and to choose the lowest sign, i.e., a negative sign for the D value of the real S = 3/2. Further, the observation of a parallel EPR signal indicates that the rhombicity has to be different from zero to account for a nonzero transition probability. These observations are in agreement with the results obtained by the fit of the magnetic data of **1** and with previous reports on Co(iprsal)$_2$[17] (where iprsal is the anion of the *N*-isopropylsalicylaldimine Schiff base), characterized by a ligand field around the Co(II) center very close to the one observed in **1**. The ground doublet of Co(iprsal)$_2$ was indeed characterized by EPR to have g_z = 7.1, g_x = 0.6, $g_y < 0.3$, and the real g factors were estimated as g_z = 2.37 and g_{xy} = 2.26 by single-crystal magnetic measurements.

The nature of the anisotropy in **1** was further investigated by Angular Overlap Model (AOM) calculations,[18] which was shown in the past to be a powerful tool to analyze the electronic structure of distorted Co(II) complexes.[19] The calculations have been performed on a CoN_2O_2 chromophore of idealized C_{2v} symmetry taking an average of the angular coordinates of the two Co centers. The z axis was chosen as the bisector of the N−Co−O angles of the coordinating Schiff bases, while the x axis was chosen as lying in the N−Co−O plane of one of the bases. We considered as starting values of the ligand field parameters B, C, ζ, and $10Dq$, those used to model the EPR properties of Co(iprsal)$_2$, but we further considered π-interactions, which we varied between $0.1e_\sigma$ and $0.4e_\sigma$. For the nitrogen atoms, the π-interaction was further considered as confined to the direction perpendicular to the Schiff-base plane, due to the sp^2 hybridization of the imine nitrogen atom,[20] while those involving oxygen atoms were considered as isotropic. We further investigated the calculated electronic energies and effective g-factors of the ground doublet varying the $10Dq$ value between 13 500 and 16 500 cm^{-1} and allowed for reduction of the B Racah parameters down to $0.9B_0$, where B_0 = 988.6 cm^{-1} is the free ion value for Co(II).[21]

The parameter set that best simulated the experimental (UV−vis and EPR) data is reported in Table S1: this provided reasonable reproduction of the features observed in the electronic spectrum, with transitions expected in the 440−465 nm ($^4A_2 \rightarrow {}^4T_1(P)$) and in the 910−1045 nm range for the three components of the $^4A_2 \rightarrow {}^4T_1(F)$ transition in C_{2v} symmetry (see Figure S5), and effective g values for the ground doublet of g_z = 7.11, g_x = 0.66, and g_y = 0.76, in good agreement with the experimental results. The corresponding spin-Hamiltonian parameters calculated for the real S = 3/2 spin are D = −21 cm^{-1}, E/D = 0.11, g_x = 2.17, g_y = 2.10, and g_z = 2.40, confirming the expectation based on the perturbative approach of eq 2 of an easy axis anisotropy with non-negligible rhombic character. More importantly, the easy axis type anisotropy is predicted for the whole range of the parameter space investigated (see Figure S6).

As a whole, the analysis of the static magnetic properties and EPR spectroscopy of **1** clearly leads to the conclusion that both cobalt(II) centers are characterized by a large easy axis type anisotropy, with a separation between the two doublets larger than 40 cm^{-1} (being equal to 2D). These are ingredients that might lead to slow relaxation of the magnetization at low temperature and prompted us to investigate the dynamic magnetic properties of **1**.

The ac measurements under 0 G static field showed no out-of-phase signals; however, application of a dc field of 1000 Oe results in the observation of frequency-dependent χ'' signals, suggesting a SIM behavior for each cobalt(II) (Figure 6, the corresponding graph for the χ' component is shown in Figure S7). The difference in the magnetization dynamics in zero and applied external field is usually attributed to the suppression of quantum tunneling (QT) of magnetization by the dc field. Even if the mixing of the ground $M_S = \pm 3/2$ levels by rhombic anisotropy is in principle forbidden according to Kramers' theorem in half-integer spin systems, the observed behavior might be due to the mixing of $M_S = \pm 3/2$ states through hyperfine or dipolar interactions.[12a,c]

The Cole−Cole plots (χ_M'' against χ_M') at several temperatures (Figure 7) were simulated using the conventional generalized Debye model, taking into account the width of the τ distribution using α parameters ($0 \le \alpha \le 1$, the simple Debye model corresponding to α = 0). This allowed extracting the temperature dependence of the relaxation times, by which the

dx.doi.org/10.1021/ic501051q | Inorg. Chem. 2014, 53, 7738−7747

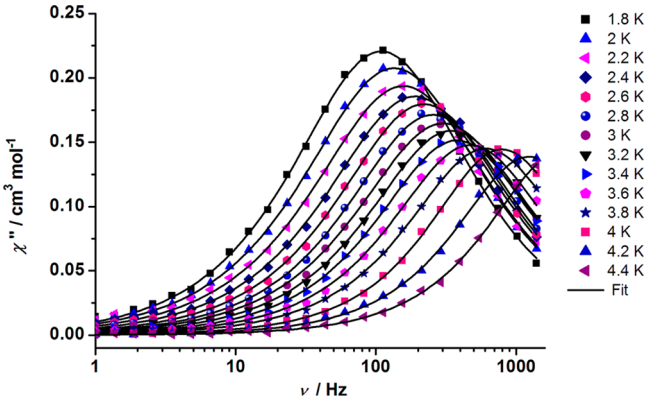

Figure 6. Frequency dependence of the out-of-phase ac susceptibility (χ'') of **1** collected at temperature intervals of 0.2 K between 1.8 and 4.4 K.

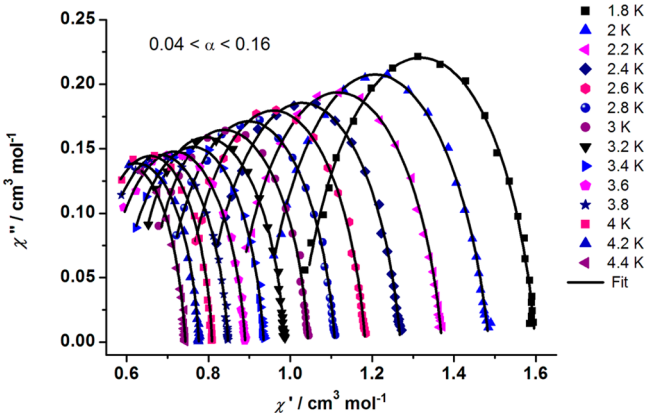

Figure 7. Cole−Cole plot for **1** at different temperatures with an applied dc field (1000 Oe) of **1**; solid lines represent the best fit.

corresponding Arrhenius plot (Figure 8) was then constructed. A thermally activated regime is observed in the higher

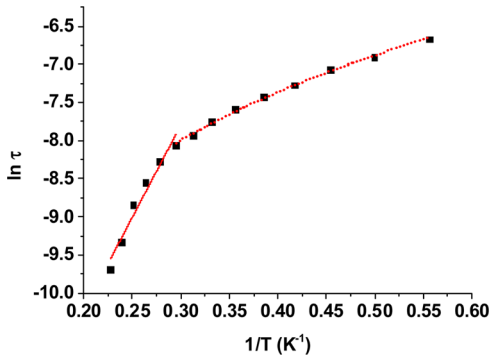

Figure 8. Arrhenius plot of the temperature dependence of the relaxation time of **1**. High-temperature data were fitted to a linear equation (continuous line), while low-temperature ones were fitted to a $\tau = aT^n$ law (dotted line). Best fit parameters are reported in the text.

temperature range, above 5 K, and the highest investigated temperatures provide for the Arrhenius law $\tau = \tau_0 \exp(\Delta/k_BT)$ the following parameters: $\tau_0 = 2.5(3) \times 10^{-7}$ s and $\Delta = 26(1)$ K. It is however quite evident that the relaxation process does not follow the simple linear behavior that would be indicative of an Orbach relaxation process, nor does it level off as it could be expected if only residual QT processes were active. Similar behavior has been reported for several different 3d and 4f mononuclear complexes, and the corresponding behavior attributed to a combination of Raman, direct, and QT relaxation paths,[22] as well as to the effect of intermolecular interactions. For this reason we investigated the magnetic properties of a $Zn_{0.98}Co_{0.02}$ sample. M vs H curves (Figure S8) could be reproduced, also in this case, only by assuming $D < 0$ (best fit parameters using the Hamiltonian eq 1: $g_\perp = 2.21(2)$, $g_\parallel = 2.36(2)$; $D = -32(2)$ cm^{-1}); X-band EPR spectra confirmed the easy axis nature of the system, with $g^{\text{eff}}{}_\parallel \approx 7.00$ and no evidence of perpendicular features in the investigated field range, suggesting $g_\perp{}^{\text{eff}} < 0.6$ (see Figure S9). Notwithstanding these features, no χ'' signal is observed, in either zero or applied field, indicating that the slow relaxation process observed in the pure sample disappears. This is completely different from what is reported in ref 22 for both easy axis and easy plane anisotropy and suggests that the slow magnetic relaxation observed in the pure compound is not intrinsic to the two tetrahedral Co centers, but is due to collective phenomena. Since dipolar-driven relaxation normally results in a slowing of the dynamics on dilution,[23] we tentatively attribute this behavior to phonon bottleneck effects. The latter have been recently reported in lanthanide-based molecular systems[24] and have been attributed to the trapping of resonant phonons. The relaxation time was found to follow a $\tau = aT^n$ dependence, where $n = -2$ is theoretically expected for this phonon bottleneck phenomenon. Accordingly we fitted the temperature dependence of the low-temperature relaxation rate of pure **1** by the same law, which provided reasonable results with a best fit exponent of -2.15 ± 0.05. Even if more detailed studies would be required to validate this hypothesis, this result is suggestive of the phonon bottleneck mechanism being the active one in promoting slow relaxation in this temperature range in the pure phase. This is also in agreement with the nonobservation of the phenomenon in the diamagnetically diluted derivative, where the phonons are able to transfer the energy of the spin bath thanks to the reduced number of spins.

As a whole, these results clearly confirm the indication of recent reports that the observation of the slow relaxation of the magnetization in single-ion systems (either 3d, 4f, or 5f) is not necessarily due to the presence of an easy axis anisotropy[22] and is not bound to it even if this is present, like in the case reported here.

Luminescence Properties of the Zinc Helicate. We performed a comparative study of the spectral characteristics (absorption, excitation, and fluorescence spectra), fluorescence quantum yield, and lifetime of compound **3** in solvents of different polarity.

The long-wavelength absorption band of the helicand is located at 333 nm, and it is due, according to literature data,[25] to $\pi-\pi^*$ transitions of the iminophenol backbone. The solvent effect on the band position is minor, i.e., a 5 nm bathochromic shift with decreasing hydrogen bond acceptor character of the solvent (Figure 9a). No helicand fluorescence emission was detected upon excitation at 333 nm.

The zinc helicate **3** exhibits an additional absorption band at around 410 nm (Figure 9b). Recently, such a band was observed by Chakraborty et al.[25] during Zn(II) ion addition to Schiff-base ligands with structure related to that of our helicand and considered as an indicator of complex formation. Upon excitation at the wavelength of absorption maximum of this band, compound **3** emits fluorescence centered at 530 nm (Figure 10a). The position of the fluorescence band is

dx.doi.org/10.1021/ic501051q | Inorg. Chem. 2014, 53, 7738−7747

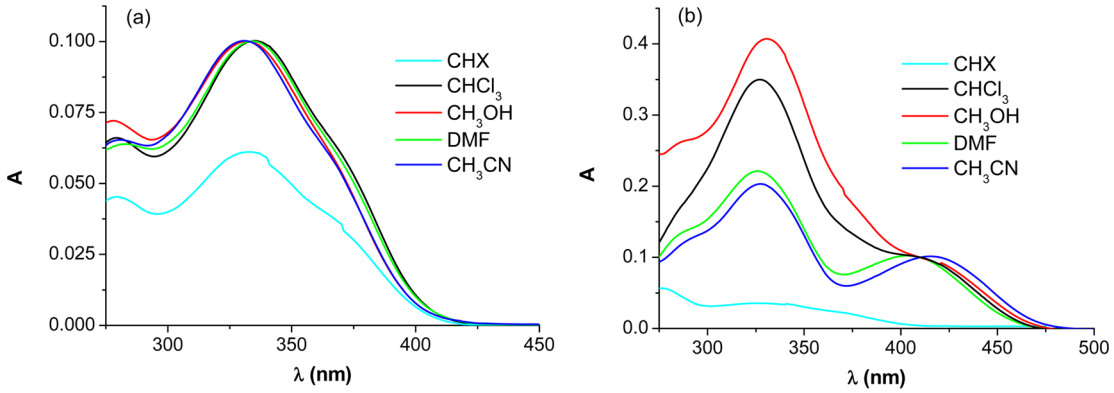

Figure 9. Absorption spectra of the (a) helicand ($A_{333\ nm}$ = 0.100 for all solvents except CHX, for which $A_{333\ nm}$ = 0.075) and (b) zinc helicate **3** ($A_{410\ nm}$ = 0.100 for all solvents except CHX, for which $A_{410\ nm}$ = 0.035).

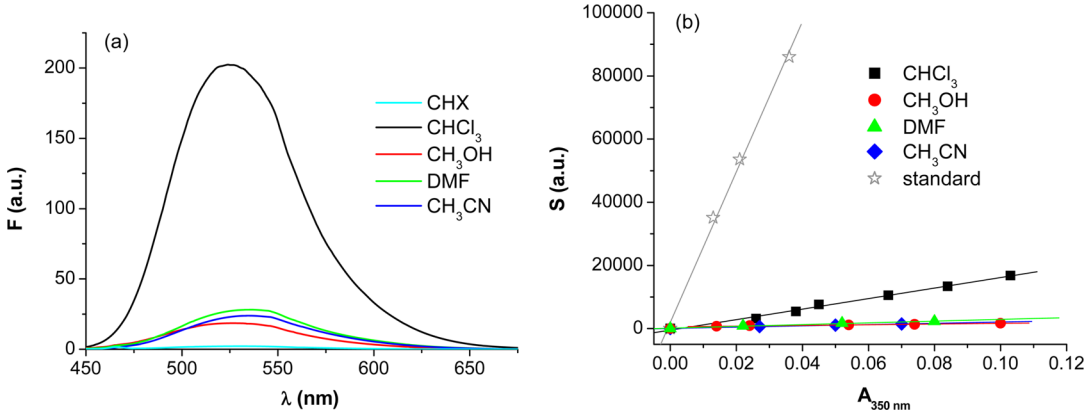

Figure 10. (a) Fluorescence spectra of the zinc helicate **3** in solvents of different polarity. (b) Plots of the integrated fluorescence intensities of compound **3** and of the quinine sulfate standard versus their absorbances at the respective absorption maxima.

Table 2. Photophysical Parameters of the Zinc Helicate 3

solvent	λ_a (nm)	λ_f (nm)	$\Delta\nu_{Stokes}$ (cm^{-1})	Φ	τ_1 (ns)	f_1[a]	τ_2 (ns)	f_2	χ^2[b]
$CHCl_3$	327; 416	525	4991	0.045	0.808	8.460	3.721	91.54	1.151
CH_3OH	326; 405	527	5716	0.003	0.425	96.68	3.418	3.318	1.371
DMF	331; 410	535	5699	0.007	0.704	84.50	3.351	15.50	1.091
CH_3CN	326; 407	535	5878	0.005	0.582	95.59	4.011	4.413	1.529

[a] $f_i = (B_i\tau_i)/(\sum_i B_i\tau_i)$ is the fractional fluorescence intensity of component i from the total intensity at λ_f. [b] χ^2 is the statistical parameter of the decay.

unaltered upon excitation with wavelengths in the range 325–425 nm. On the basis of the spectral features, namely, the large Stokes shifts (5000–6000 cm^{-1}, Table 2) and the structureless profile of the band, the origin of the fluorescence emission of compound **3** is ascribed to $\pi^*-\pi$ transitions of the metal-perturbed ligand.[8b] It is known that emission from metal-centered excited states is highly unlikely for Zn(II) complexes, since the ion is in its stable d^{10} configuration.[26] Enhancement in ligand fluorescence upon coordination can be explained by the increased conformational rigidity of the ligand within the complex, leading to a smaller degree of nonradiative deactivation.[27]

The excitation spectra of the zinc helicate **3** consist of two bands centered at 325 and 415 nm and match its absorption spectra. This is exemplified in Figure 11 for the case of chloroform as a solvent. Such similarity between excitation and absorption spectra concerning band positions and intensity ratios has also been reported for other recently synthesized metal complexes[28] and is considered an indication of the fact that no geometry change occurs upon excitation.[29]

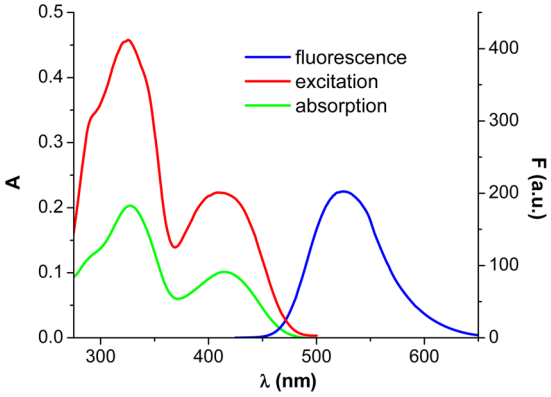

Figure 11. Absorption, excitation, and fluorescence spectra of compound **3** in chloroform. λ_{ex} = 416 nm; λ_{em} = 525 nm.

Differently from the absorption case, the fluorescence emission of compound **3** depends strongly on the nature of the solvent, indicating specific solvation in the excited state. To

dx.doi.org/10.1021/ic501051q | Inorg. Chem. 2014, 53, 7738–7747

obtain quantitative data on this dependence, the fluorescence quantum yield (which reflects the extent of radiative/non-radiative deactivation processes) and the fluorescence lifetime (the average time spent by the molecule in an excited state before emitting fluorescence) have been determined. The Φ_X values were calculated on the basis of the plots in Figure 10b, the highest value being 4.47%, in chloroform (Table 2). The low solubility of compound **3** in cyclohexane did not allow quantitative determinations in this solvent. The fluorescence decay profiles of the zinc helicate **3** are depicted in Figure 12,

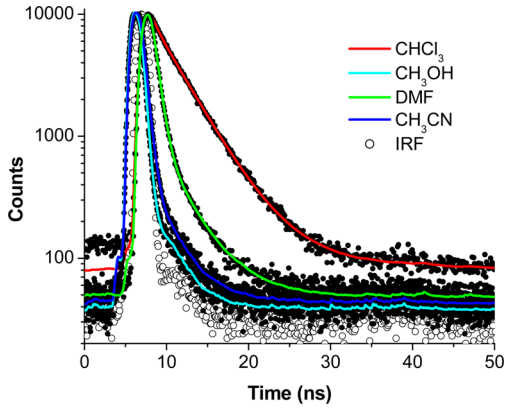

Figure 12. Fitted fluorescence intensity decays of the zinc helicate **3** in different solvents. λ_{ex} = 375.6 nm; λ_{em} = 525 nm ($CHCl_3$, CH_3OH) and 535 nm (DMF, CH_3CN). IRF denotes the instrument response function.

the corresponding τ values being listed in Table 2. The decays are characterized by two lifetimes: a long component of ~4 ns, which is predominant in chloroform and is responsible for the stronger emission in this solvent, and a shorter component of ~0.7 ns, predominant in the other solvents.

CONCLUSIONS

The helicand resulting from the 2:1 condensation reaction between *o*-vanillin and 4,4′-diaminodiphenyl ether provides three new double-stranded helicates containing Co(II), Cu(II), and Zn(II) ions, respectively. Within the three compounds, the metal ions display distorted tetrahedral coordination geometries. The most interesting compound, from the magnetic point of view, is the cobalt(II) derivative: EPR spectroscopy indicates an easy axis type magnetic anisotropy, with some rhombicity, for both Co^{II} centers, and dynamic susceptibility measurements provide evidence that the magnetization relaxes slowly under the application of a small dc field. To the best of our knowledge, this is the first example of a helicate containing a transition metal ion showing this behavior. In contrast with what is commonly assumed, however, dilution experiments demonstrated that the slow relaxation cannot be attributed to the magnetic anisotropy barrier, even if the magnetic data analysis unequivocally shows this is present, but rather to phonon bottleneck effects. The use of different metal ions to assemble helicates is appealing when looking for various physical properties. For example, the zinc helicate shows luminescence in solution, which depends strongly on the nature of the solvent. The highest quantum yield (4.47%) was observed in chloroform, with a lifetime of 4 ns.

EXPERIMENTAL SECTION

General Procedures. Reactions were carried out under a normal atmosphere and with solvents of commercial purity. The IR spectra were recorded on KBr pellets with a Bruker Tensor 37 spectrometer in the 4000−400 cm^{-1} range. The UV−vis NIR was recorded with a V-670 Jasco spectrophotometer in the 2000−200 nm range.

Syntheses. *H_2L.* A methanolic solution of bis(4-aminophenyl) ether (2 g, 10 mmol) was added to a stirred solution of 3-methoxysalicylaldehyde (3.1 g, 20 mmol) in methanol (100 mL). The mixture was stirred under heating at 50 °C for several hours. The resulting orange precipitate was filtered off, washed with a small amount of methanol, and dried. Yield: 90%.

*$[Co_2L_2]$·3DMF, **1**.* Triethylamine (2 mmol, 0.28 mL) was added to a stirred suspension of H_2L (1 mmol, 0.548 g) in an acetonitrile/methanol mixture (2:1, 30 mL). The clear yellowish-orange solution was reacted with a methanolic solution of $Co(ClO_4)_2·6H_2O$ (1 mmol, 0.365 g). After a few minutes, a red microcrystalline precipitate appeared, which was isolated by filtration, washed with methanol, allowed to air-dry, and then dissolved in a small amount of DMF. The slow evaporation of the resulting solution at room temperature afforded red single crystals of complex **1**. Yield: 71%. IR data (KBr,

Table 3. Crystallographic Data and Details of Data Collection and Structure Refinement Parameters

	1	2	3
chemical formula	$C_{65}H_{65}Co_2N_7O_{13}$	$C_{59}H_{51.8}Cu_2N_5O_{11.4}$	$C_{65}H_{65}Zn_2N_7O_{13}$
fw (g/mol)	1270.10	1140.34	1282.98
cryst syst	monoclinic	tetragonal	monoclinic
space group	$P2_1/c$	$P4_2/n$	$P2_1/c$
a (Å)	15.0569(7)	14.2756(7)	15.0884(6)
b (Å)	13.7433(6)	14.2756(7)	13.7579(6)
c (Å)	30.4285(17)	27.1417(14)	30.3069(13)
α (deg)	90.00	90.00	90.00
β (deg)	92.452(4)	90.00	92.14
γ (deg)	90.00	90.00	90.00
volume (Å^3), Z	6290.8(5), 4	5531.3(5), 8	6286.9(5), 4
temperature (K)	293(2)	293(2)	293(2)
calcd density (Mg m^{-3})	1.341	1.369	1.355
absorption coeff (mm^{-1})	0.596	0.834	0.831
final R indices [$I > 2\sigma(I)$]	R_1 = 0.0490; wR_2 = 0.0879	R_1 = 0.0781; wR_2 = 0.1867	R_1 = 0.0549; wR_2 = 0.1218
R indices (all data)	R_1 = 0.1644; wR_2 = 0.1118	R_1 = 0.1305; wR_2 = 0.2193	R_1 = 0.1087; wR_2 = 0.1466
goodness-of-fit on F^2	0.776	1.029	0.920
$\Delta\rho_{min}$ and $\Delta\rho_{max}$ (e Å^{-3})	0.388 and −0.214	0.934 and −0.483	0.540 and −0.300

dx.doi.org/10.1021/ic501051q | Inorg. Chem. 2014, 53, 7738−7747

cm^{-1}): 1668.2(m), 1605.91(m), 1541.78(w), 1494.94(s), 1434.79(m), 1386.54(w), 1237.25(s), 1187.49(s), 859.97(w). Anal. Calcd: C, 61.47; H, 5.16; N, 7.72. Found: C, 60.98; H, 5.33; N, 7.98.

$[Cu_2L_2]\cdot DMF\cdot 0.4H_2O$, **2**. Triethylamine (2 mmol, 0.28 mL) was added to a stirred suspension of H_2L (1 mmol, 0.548 g) in methanol (2:1, 30 mL). The clear yellowish-orange solution was reacted with a methanolic solution of $Cu(ClO_4)_2\cdot 6H_2O$ (1 mmol, 0.370 g). After several days dark brown crystals appeared, which were isolated by filtration, washed with methanol, allowed to air-dry, and then dissolved in a small amount of DMF/methanol mixture (2:1). Slow evaporation of the new solution, at room temperature, yielded crystals suitable for X-ray measurements. Yield: 45%. IR data (KBr, cm^{-1}): 1609.41(s), 1543.91(m), 1494.51(s), 1447.67(m), 1436.99(m), 1238.99(s), 1187.64(s), 858.43(w). Anal. Calcd: C, 62.14; H, 4.58; N, 6.14. Found: C, 61.87; H, 4.82; N, 6.31.

$[Zn_2L_2]\cdot 3DMF$, **3**. Triethylamine (2 mmol, 0.28 mL) was added to a stirred suspension of H_2L (1 mmol, 0.548 g) in an acetonitrile/methanol mixture (2:1, 30 mL). The formed clear yellowish-orange solution was reacted with a methanolic solution of $Zn(ClO_4)_2\cdot 6H_2O$ (1 mmol, 0.372 g). After a few minutes, a light yellow microcrystalline precipitate appeared, which was isolated by filtration, washed with methanol, allowed to air-dry, and then dissolved in a small amount of DMF. The slow evaporation of the resulting solution at room temperature afforded light yellow single crystals. Yield: 65%. IR data (KBr, cm^{-1}): 1668.42(m), 1609.27(m), 1542.59(w), 1496.35(m), 1463.86(m), 1438.39(m), 1386.58(w), 1237.09(s), 1187.81(s), 859.84(w). Anal. Calcd: C, 60.85; H, 5.11; N, 7.64. Found: C, 60.63; H, 5.29; N, 7.52.

The doped derivative $Zn_{0.98}Co_{0.02}$ was prepared by a similar procedure to that for compounds **1** and **3**, but using a mixture of $Zn(ClO_4)_2\cdot 6H_2O$ and $Co(ClO_4)_2\cdot 6H_2O$ prepared in a 0.98:0.02 molar ratio. The obtained doped level in the final product was tested by elemental analysis and magnetic measurements (Figure S8), while an X-band EPR spectrum was used to test the persistence of the effective g value of the Co(II) ions (Figure S9).

X-ray Structure Determinations. Details about data collection and solution refinement are given in Table 3. X-ray diffraction measurements were performed on a STOE IPDS II diffractometer operating with a Mo Kα (λ = 0.71073 Å) X-ray tube with graphite monochromator for complexes **1** and **3** and on an Xcalibur Eos diffractometer operating with Mo Kα (λ = 0.71073 Å) X-ray tube with graphite monochromator for complex **2**. The structures were solved (SHELXS-97) by direct methods and refined (SHELXL-97) by full-matrix least-squares procedures on F^2.[30] All non-H atoms of the donor molecules were refined anisotropically, and hydrogen atoms were introduced at calculated positions (riding model), included in structure factor calculations, but not refined. Crystallographic data for the structures have been deposited in the Cambridge Crystallographic Data Centre, deposition numbers CCDC 1000206−1000208. These data can be obtained free of charge from the Cambridge Crystallographic Data Centre via www.ccdc.cam.ac.uk/data_request/cif.

Spectral Measurements. Solutions of helicand and compound **3** were prepared in nonpolar (cyclohexane, CHX), weakly polar (chloroform), polar protic (methanol), and polar aprotic (dimethylformamide (DMF), acetonitrile) solvents. All solvents were from Sigma-Aldrich and were used without further purification. Electronic absorption spectra of the solutions were recorded on a V-560 Jasco UV−vis spectrophotometer at 298 K, and the absorbance of each solution was noted at the wavelength of fluorescence excitation. Steady-state fluorescence and excitation spectra were then collected on an FP-6300 Jasco spectrofluorimeter at 298 K for solutions having absorbance below 0.1, in order to avoid inner-filter effects at and above the excitation wavelength.

The fluorescence quantum yield of the zinc helicate **3** has been estimated with respect to the quantum yield of a standard of quinine sulfate in 0.5 M sulfuric acid, according to eq 3,[31]

$$\Phi_X = \Phi_{std}\left(\frac{grad_X}{grad_{std}}\right)\left(\frac{{n_X}^2}{{n_{std}}^2}\right) \quad (3)$$

where subscripts X and std denote compound **3** and the standard, respectively, Φ is the fluorescence quantum yield (Φ_{std} = 0.55 at 298 K),[32] grad is the gradient of a plot of integrated fluorescence intensity (S) versus absorbance (A) at the excitation wavelength, and n is the refractive index of the solvent (i.e., $CHCl_3$: 1.446; CH_3OH: 1.329; DMF: 1.431; CH_3CN: 1.344; sulfuric acid 0.5 M: 1.340[33]).

Fluorescence lifetimes of compound **3** were obtained with a time-correlated single photon counting FLS920 system from Edinburgh Instruments equipped with a picosecond-pulsed diode laser (λ_{ex} = 375.6 nm). The fluorescence decays were fitted by reconvolution analysis using a biexponential function, according to eq 4,[31]

$$F(t) = A + \sum_i B_i e^{-t/\tau_i} \quad (4)$$

where $F(t)$ is the time-dependent fluorescence intensity, τ_i the characteristic fluorescence lifetime, and B_i is the pre-exponential factor.

Magnetic Measurements. The W-band EPR spectrum of **1** was acquired by using a Bruker E600 spectrometer with a cylindrical cavity operating at around 94 GHz, equipped with a split-coil superconducting magnet (Oxford Instruments) and a continuous flow cryostat to work at low temperature (CF935 Oxford Instruments). The powder was ground and blocked with grease to avoid preferential orientation in field. The X-band EPR spectra of $Zn_{0.98}Co_{0.02}$ were obtained by a Bruker E500 spectrometer equipped with a continuous flow ^{4}He cryostat (ESR900) to work at low temperature.

Isothermal magnetization of **1** was measured by using a VSM PPMS Quantum Design magnetometer. The dynamic magnetic characterization of $Zn_{0.98}Co_{0.02}$ was measured using a PPMS magnetometer from Quantum Design equipped with the ac measurement system (ACMS) option. The static magnetization of $Zn_{0.98}Co_{0.02}$ was measured on an MPMS Quantum Design SQUID magnetometer. The reported values were obtained by subtracting the diamagnetic contribution of the sample holder, measured in the same temperature and field range, and the large intrinsic contribution of the diamagnetic host estimated by Pascal's constant.

■ ASSOCIATED CONTENT

Supporting Information

This material is available free of charge via the Internet at http://pubs.acs.org.

■ AUTHOR INFORMATION

Corresponding Authors

*E-mail: marius.andruh@dnt.ro.
*E:mail: Floriana.Tuna@manchester.ac.uk.
*E-mail: lorenzo.sorace@unifi.it.

Notes

The authors declare no competing financial interest.

■ ACKNOWLEDGMENTS

The financial support of the Italian and Romanian foreign affair secretariat through the project Multifunctional Molecular Nanosystems is gratefully acknowledged.

■ DEDICATION

This paper is dedicated to our friend, Professor Miguel A. Novak, on the occasion of his 60th birthday.

■ REFERENCES

(1) (a) Constable, E. C. *Chem. Ind.* **1994**, 56. (b) Constable, E. C. In Lehn, J.-M.; Atwood, L. Davis, J. E. D.; MacNicol, D. D.; Vögtle, F., Eds. *Comprehensive Supramolecular Chemistry*; Oxford: Pergamon, 1996; Vol. 9, p 213. (c) Leininger, S.; Olenyuk, B.; Stang, P. J. *Chem. Rev.* **2000**, *100*, 853. (d) Holliday, B. J.; Mirkin, C. A. *Angew. Chem., Int. Ed.* **2001**, *40*, 2022. (e) Lehn, J.-M. *Supramolecular Chemistry—Concepts and Perspectives*; VCH: Weinheim, 1995.

(2) (a) Piguet, C.; Bernardinelli, G.; Hopfgartner, G. *Chem. Rev.* **1997**, *97*, 2005. (b) Albrecht, M. *Chem. Soc. Rev.* **1998**, *27*, 281. (c) Albrecht, M. *Chem. Rev.* **2001**, *101*, 3457. (d) Hannon, M. J.; Childs, L. J. *Supramol. Chem.* **2004**, *16*, 7. (e) Piguet, C.; Borkovec, M.; Hamacek, J.; Zeckert, K. *Coord. Chem. Rev.* **2005**, *249*, 705.

(3) (a) Lehn, J.-M. *Chem.—Eur. J.* **2000**, *6*, 2097. (b) Lehn, J.-M. *Science* **2002**, *295*, 2400.

(4) See, for example: (a) Hamblin, J.; Jackson, A.; Alcock, N. W.; Hannon, M. J. *J. Chem. Soc., Dalton Trans.* **2002**, 1635. (b) Hong, M.; Cheng-jie, F.; Chun-ying, D.; Yu-ting, L.; Qing-jin, M. *Dalton Trans.* **2003**, 1229. (c) Albrecht, M.; Janser, I.; Kamptmann, S.; Weis, P.; Wibbeling, B.; Fröhlich, R. *Dalton Trans.* **2004**, 37. (d) Gupta Sreerma, S.; Pal, S. *Inorg. Chem.* **2005**, *44*, 6299. (e) Cucos, P.; Pascu, M.; Sessoli, R.; Avarvari, N.; Pointillart, F.; Andruh, M. *Inorg. Chem.* **2006**, *45*, 7035.

(5) See, for example: (a) Yoshida, N.; Oshio, H.; Ito, T. *Chem. Commun.* **1998**, 63. (b) Yoshida, N.; Ichikawa, K. *Chem. Commun.* **1997**, 1091. (c) Archer, R. J.; Hawes, C. S.; Jameson, G. N. L.; McKee, V.; Moubaraki, B.; Chilton, N. F.; Murray, K. S.; Schmitt, W.; Kruger, P. E. *Dalton Trans.* **2011**, *40*, 12368. (d) Song, Y.; Koval, I. A.; Gamez, P.; van Albada, G. A.; Mutikainen, I.; Turpeinen, U.; Reedijk, J. *Polyhedron* **2004**, *23*, 1769. (e) Şengül, A.; Wang, W. J.; Coles, S. J. *Polyhedron* **2009**, *28*, 69. (f) Chu, Z.; Huang, W. *J. Mol. Struct.* **2007**, *837*, 15. (g) Kruger, P. E.; Martin, N.; Nieuwenhuyzen, M. *J. Chem. Soc., Dalton Trans.* **2001**, 1966. (h) Yoshida, N.; Oshio, H.; Ito, T. *J. Chem. Soc., Perkin Trans. 2* **1999**, 975. (i) Sreerama, S. G.; Mukhopadhyay, A.; Pal, S. *Polyhedron* **2007**, *26*, 4101. (j) Ronson, T. K.; Adams, H.; Ward, M. D. *Inorg. Chim. Acta* **2005**, *358*, 1943. (k) Vázquez, M.; Taglietti, A.; Gatteschi, D.; Sorace, L.; Sangregorio, C.; González, A. M.; Maneiro, M.; Pedrido, R. M.; Bermejo, M. R. *Chem. Commun.* **2003**, 1840.

(6) (a) Novitchi, G.; Costes, J. P.; Tuchagues, J. P.; Vendier, L.; Wernsdorfer, W. *New J. Chem.* **2008**, *32*, 197. (b) Novitchi, G.; Costes, J. P.; Tuchagues, J. P. *Dalton Trans.* **2004**, 1739.

(7) (a) Floquet, S.; Ouali, N.; Bocquet, B.; Bernardinelli, G.; Imbert, D.; Bünzli, J. C. G.; Hopfgartner, G.; Piguet, C. *Chem.—Eur. J.* **2003**, *9*, 8. (b) Albrecht, M. *Z. Anorg. Allg. Chem.* **2010**, *636*, 2198. (c) Albrecht, M.; Osetska, O.; Bünzli, J. C. G.; Gumy, F.; Fröhlich, R. *Chem.—Eur. J.* **2009**, *15*, 8791. (d) Vandevyver, C. D. B.; Chauvin, A.-S.; Comby, S.; Bünzli, J. C. G. *Chem. Commun.* **2007**, 1716. (e) Fernández-Moreira, V.; Song, B.; Sivagnanam, V.; Chauvin, A.-S.; Vandevyver, C. D. B.; Gijs, M.; Hemmilä, I.; Lehr, H.-A.; Bünzli, J. C. G. *Analyst* **2010**, *135*, 42. (f) Chauvin, A.-S.; Comby, S.; Baud, M.; De Piano, C.; Duhot, C.; Bünzli, J. C. G. *Inorg. Chem.* **2009**, *48*, 10687. (g) Elhabiri, M.; Scopelliti, R.; Bünzli, J. C. G.; Piguet, C. *J. Am. Chem. Soc.* **1999**, *121*, 10747. (h) Stomeo, F.; Lincheneau, C.; Leonard, J. P.; O'Brien, J. E.; Peacock, R. D.; McCoy, C. P.; Gunnlaugsson, T. *J. Am. Chem. Soc.* **2009**, *131*, 9636. (i) Eliseeva, S. V.; Auböck, G.; van Mourik, F.; Cannizzo, A.; Song, B.; Deiters, E.; Chauvin, A.-S.; Chergui, M.; Bünzli, J. C. G. *J. Phys. Chem. B* **2010**, *114*, 2932.

(8) (a) Bullock, S. J.; Felton, C. E.; Fennessy, R. V.; Harding, L. P.; Andrews, M.; Pope, S. J. A.; Rice, C. R.; Riis-Johannessen, T. *Dalton Trans.* **2009**, 10570. (b) Zhu, A.-X.; Zhang, J.-P.; Lin, Y.-Y.; Chen, X.-M. *Inorg. Chem.* **2008**, *47*, 7389. (c) Xuan, W.; Zhang, M.; Liu, Y.; Chen, Z.; Cui, Y. *J. Am. Chem. Soc.* **2012**, *134*, 6904.

(9) Tuna, F.; Lees, M. R.; Clarkson, G. J.; Hannon, M. J. *Chem.—Eur. J.* **2004**, *10*, 5737.

(10) (a) Habib, F.; Murugesu, M. *Chem. Soc. Rev.* **2013**, *42*, 3278. (b) Woodruff, D. N.; Winpenny, R. E. P.; Layfield, R. A. *Chem. Rev.* **2013**, *113*, 5110.

(11) Xu, H.-W.; Li, J.-X.; Li, Y.-H. *Acta Crystallogr.* **2008**, *E64*, o1145.

(12) (a) Zadrozny, J. M.; Long, J. R. *J. Am. Chem. Soc.* **2011**, *133*, 20732. (b) Zadrozny, J. M.; Liu, J.; Piro, N. A.; Chang, C. J.; Hill, S.; Long, J. R. *Chem. Commun.* **2012**, *48*, 3927. (c) Yang, F.; Zhou, Q.; Zhang, Y. Q.; Zeng, G.; Li, G. H.; Shi, Z.; Wang, B. W.; Feng, S. H. *Chem. Commun.* **2013**, *49*, 5289. (d) Valejo, J.; Castro, I.; Ruiz-Garcia, R.; Cano, J.; Julve, M.; Lloret, F.; de Munno, G.; Wernsdorfer, W.; Pardo, E. *J. Am. Chem. Soc.* **2012**, *134*, 15704.

(13) (a) Murrie, M. *Chem. Soc. Rev.* **2010**, *39*, 1986. (b) Caneschi, A.; Gatteschi, D.; Lalioti, N.; Sangregorio, C.; Sessoli, R.; Venturi, G.; Vindigni, A.; Rettori, A.; Pini, M. G.; Novak, M. A. *Angew. Chem., Int. Ed.* **2001**, *40*, 1760. (c) Caneschi, A.; Gatteschi, D.; Lalioti, N.; Sessoli, R.; Sorace, L.; Tangoulis, V.; Vindigni, A. *Chem.—Eur. J.* **2002**, *8*, 286. (d) Miyasaka, H.; Julve, M.; Yamashita, M.; Clérac, R. *Inorg. Chem.* **2009**, *48*, 3420.

(14) (a) Jurca, T.; Farghal, A.; Lin, P.-H.; Korobkov, I.; Murugesu, M.; Richeson, D. S. *J. Am. Chem. Soc.* **2011**, *133*, 15814. (b) Zhu, Y.-Y.; Cui, C.; Zhang, Y.-Q.; Jia, J.-H.; Guo, X.; Gao, C.; Qian, K.; Jiang, S.-D.; Wang, B.-W.; Wang, Z.-M.; Gao, S. *Chem. Sci.* **2013**, *4*, 1802. (c) Huang, W.; Liu, T.; Wu, D.; Cheng, J.; Ouyang, Z. W.; Duan, C. *Dalton Trans.* **2013**, *42*, 15326.

(15) (a) Tregenna-Piggott, P. L. W. *MagProp* (part of the NIST DAVE software suite), v2.2 (Aug 20, 2013). http://www.ncnr.nist.gov/dave. (b) Chilton, N. F.; Anderson, R. P.; Turner, L. D.; Soncini, A.; Murray, K. S. *J. Comput. Chem.* **2013**, *34*, 1164.

(16) (a) Banci, L.; Bencini, A.; Benelli, C.; Gatteschi, D. *Nouv. J. Chim.* **1980**, *4*, 593. (b) Pilbrow, J. R. *J. Magn. Reson.* **1978**, *31*, 479.

(17) Horrocks, W. DeW., Jr.; Burlone, D. A. *Inorg. Chim. Acta* **1979**, *35*, 165.

(18) Bencini, A.; Ciofini, I.; Uytterhoeven, M. G. *Inorg. Chim. Acta* **1998**, *274*, 90.

(19) (a) Gerloch, M.; McMeeking, R. F. *J. Chem. Soc., Dalton Trans.* **1975**, 2443. (b) Banci, L.; Bencini, A.; Benelli, C.; Gatteschi, D.; Zanchini, C. *Struct. Bonding (Berlin)* **1982**, *52*, 37. (c) Bencini, A.; Beni, A.; Costantino, F.; Dei, A.; Gatteschi, D.; Sorace, L. *Dalton Trans.* **2006**, 722.

(20) Cruse, D. A.; Gerloch, M. *J. Chem. Soc., Dalton Trans.* **1977**, 152.

(21) Brorson, M.; Schäffer, C. E. *Inorg. Chem.* **1988**, *27*, 2522.

(22) (a) Zadrozny, J. M.; Atanasov, M. A.; Bryan, M.; Lin, C.-Y.; Rekken, B. D.; Power, P. P.; Neese, F.; Long, J. R. *Chem. Sci.* **2013**, *4*, 125. (b) Liu, J.-L.; Yuan, K.; Leng, J.-D.; Ungur, L.; Wernsdorfer, W.; Guo, F.-S.; Chibotaru, L. F.; Tong, M.-L. *Inorg. Chem.* **2012**, *51*, 8538. (c) Lucaccini, E.; Sorace, L.; Perfetti, M.; Costes, J.-P.; Sessoli, R. *Chem. Commun.* **2014**, *50*, 1648.

(23) (a) Luis, F.; Martìnez- Peréz, M. J.; Montero, O.; Coronado, E.; Cardona-Serra, S.; Martì-Gastaldo, C.; Clemente-Juan, J. M.; Ses, J.; Drung, D.; Schurig, T. *Phys. Rev. B* **2010**, *82*, 060403. (b) Car, P.-E.; Perfetti, M.; Mannini, M.; Favre, A.; Caneschi, A.; Sessoli, R. *Chem. Commun.* **2011**, *47*, 3751−3753. (c) Vergnani, L.; Barra, A.-L.; Neugebauer, P.; Rodriguez-Douton, M. J.; Sessoli, R.; Sorace, L.; Wernsdorfer, W.; Cornia, A. *Chem.−Eur. J.* **2012**, *18*, 3390.

(24) (a) Rossin, A.; Giambastiani, G.; Peruzzini, M.; Sessoli, R. *Inorg. Chem.* **2012**, *51*, 6962. (b) Orendáč, M.; Sedláková, L.; Čižmár, E.; Orendáčová, A.; Feher, A.; Zvyagin, S. A.; Wosnitza, J.; Zhu, W. H.; Wang, Z. M.; Gao, S. *Phys. Rev. B* **2010**, *81*, 214410. (c) Lopez, N.; Prosvirin, A. V.; Zhao, H. H.; Wernsdorfer, W.; Dunbar, K. R. *Chem.—Eur. J.* **2009**, *15*, 11390.

(25) Chakraborty, B.; Halder, P.; Chakraborty, S.; Das, O.; Paria, S. *Inorg. Chim. Acta* **2012**, *387*, 332.

(26) Ji, Y.-F; Wang, R.; Ding, S.; Du, C.-F.; Liu, Z.-L. *Inorg. Chem. Commun.* **2012**, *16*, 47.

(27) Basak, S.; Sen, S.; Banerjee, S.; Mitra, S.; Rosair, G.; Rodriguez, M. T. G. *Polyhedron* **2007**, *26*, 5104.

(28) (a) Nuñez, C.; Fernandez-Lodeiro, J.; Dinis, M.; Larguinho, M.; Capelo, J. L.; Lodeiro, C. *Inorg. Chem. Commun.* **2011**, *14*, 831. (b) Deiters, E.; Eliseeva, S. V.; Bünzli, J. C. G. *Front. Chem.* **2013**, *1*, 15.

(29) Gümrükçü, G.; Karaoğlan, G. K.; Erdoğmuş, A.; Gül, A.; Avcıata, U. *Dyes Pigm.* **2012**, *95*, 280.

(30) Sheldrick, G. M. *Programs for the Refinement of Crystal Structures*; University of Göttingen: Göttingen, Germany, 1996.

(31) Valeur, B. *Molecular Fluorescence. Principles and Aplications*; Wiley-VCH: Weinheim, Germany, 2002; pp 155−199.

(32) Melhuish, W. A. *J. Phys. Chem.* **1961**, *65*, 229.

(33) Dean, J. A. *Lange's Handbook of Chemistry*, 15th ed., McGraw-Hill Professional: USA, 1999; p 11.